

FORMATION AND EVOLUTION OF GALACTIC HALOS IN CLUSTERS OF GALAXIES

TAKASHI OKAMOTO AND ASAOK HABE

Hokkaido University, Sapporo 060, Japan; okamoto@phys.hokudai.ac.jp

Received 1998 March 27; accepted 1998 December 14

ABSTRACT

We investigate effects of time evolution of a rich cluster of galaxies on its member galactic halos in the standard cold dark matter (SCDM) universe using high resolution N -body simulations. We identify several hundred galactic halos within the virial radius of our simulated cluster. We also find that a large number of halos have been tidally disrupted at $z = 0$. Therefore we improve a method of deriving merging history trees of galaxies taking account of tidally stripped galaxies. The main results are as follows: (1) At high redshift ($z \simeq 2$), the mass function of the galactic halos that are in the cluster at $z = 0$ is very similar to that obtained in the field region and agrees well with the Press-Schechter mass function. (2) The mass function of cluster galaxies that consist of both galactic halos and tidally stripped galaxies has hardly evolved since $z \simeq 2$. This mass function at $z = 0$ is well represented by the Press-Schechter mass function at $z = 2$. (3) At high redshift ($z > 3$), in the region that becomes the cluster, the fraction of galaxies that have undergone recent merger is larger than that in the field. After $z \sim 3$, however, it rapidly decreases and becomes smaller than that in the field. (4) The fraction of strongly stripped galaxies among the cluster galaxies begins to increase from $z \simeq 0.5$. At $z = 0$, a clear correlation appears between this fraction and the distance from the center of the cluster. (5) Tidally truncated halos have steeper outer profiles than those of the model of Navarro, Frenk, & White.

Subject headings: galaxies: clusters: general — galaxies: halos — galaxies: interactions

1. INTRODUCTION

It is well established that galaxy populations vary with the density of neighboring galaxies in clusters of galaxies (Dressler 1980) and depend on distance from the center of clusters of galaxies (Whitmore, Gilmore, & Jones 1993). The increase in the fraction of blue, star-forming cluster galaxies with redshift (Butcher & Oemler 1978, 1984a, 1984b) also has been well established. Several physical processes have been proposed to explain these effects, including shocks induced by ram pressure from the intracluster medium (Bothun & Dressler 1986; Gavazzi & Jaffe 1987), effects of cluster tidal field (Byrd & Valtonen 1990), galaxy-galaxy interactions (Barnes & Hernquist 1991; Moore et al. 1996b; Moore, Lake, & Katz 1998b), and mergers of individual galaxies in the hierarchical clustering universe (Kauffmann, White, & Guiderdoni 1993; Kauffmann 1995a, 1995b, 1996; Baugh, Cole, & Frenk 1996).

The purpose of our study is to investigate effects of galaxy-galaxy and galaxy-cluster interactions on cluster member galaxies and to investigate when these interactions become important during the cluster evolution. As the first step for this purpose, we make cosmological N -body simulations and study how and when galactic dark halos are affected by these interactions. In particular, we pay our attention to evolution of large galactic halos ($M_h \geq 10^{11} M_\odot$).

Unfortunately, previous almost dissipationless numerical simulations have been failing to follow the evolution of galactic halos in dense environments such as galaxy groups and clusters owing to their low-resolution (White 1976; van Kampen 1995; Summers, Davis, & Evrard 1995; Moore, Katz, & Lake 1996a).

To avoid this apparent erasing of substructures in the dense environments known as the “overmerging problem,” many approaches have been taken. For example, Couchman & Carlberg (1992) tagged particles in galactic halos before a cluster forms, then applied a halo-finding algo-

rithm only for the tagged particles at final epoch. Another idea is to introduce “artificial cooling” in a collisionless simulation by collecting particles in their collapsing regions into more massive superparticles (van Kampen 1995). By these approaches, however, we cannot explore strength of galaxy-galaxy and galaxy-cluster interactions. Therefore, we use high-resolution N -body simulations and the improved method of tracing galaxies to investigate those interactions.

We should consider hydrodynamic processes of baryonic component, because radiative cooling allows baryonic component to sink into the center of a dark matter halo, where it forms a compact and tightly bound stellar system which is hardly destroyed by the tidal force and helps its host halo to survive to some degree (Summers et al. 1995). However, hydrodynamic simulations, e.g., smoothed particle hydrodynamics (SPH) simulations, need much more CPU time than the collisionless simulation. Then, it is difficult to perform wide dynamical range simulations by this approach.

Therefore, we restrict ourselves to follow evolution of dark matter halos. We trace not only surviving halos but also strongly stripped halos which may survive as galaxies if hydrodynamic processes are considered, because we find many strongly stripped halos in a cluster of galaxies in our simulation.

Recently, Ghigna et al. (1998) have reported results of simulations similar to ours, independently. However, there are two large differences between our study and theirs. The first difference is that the mass of their cluster is about half the mass of ours. Therefore, our galactic halos suffer influence of denser environment, and our cluster forms at lower redshift than theirs. The second difference is that they investigated the evolution of the cluster halos from $z = 0.5$ to $z = 0$. On the other hand, we investigate it before the formation epoch of galactic halos to present time. Clearly, our investigation gives more information about galaxy-galaxy

and galaxy-cluster interactions that affect evolution of galaxies.

In § 2 we present the method of numerical simulations, our halo-finding algorithm, and the algorithm to create halo merging history trees. The algorithm to create halo merging history trees is improved to handle the galactic halos in very dense environments. Our results are presented in § 3 and are discussed in § 4.

2. SIMULATION

2.1. The Simulation Data Set

We first describe two simulations used in this paper, and their specific purpose. The overall parameters and mass of the most massive virialized objects at $z = 0$ in both simulations are listed in Table 1. The background model for both simulations is the standard cold dark matter (SCDM) universe with the Hubble constant $H_0 = 100 h \text{ km s}^{-1} \text{ Mpc}^{-1}$, where $h = 0.5$. This model is normalized with $\sigma_8 = 1/b$, where $b = 1.5$.

Simulation A represents an average piece of the universe corresponding to the “field” environment within a sphere of radius 7 Mpc, and we use it to check our halo-finding algorithm and compare with another simulation.

In simulation B, we adopt the constrained random field method to generate the initial density perturbation field in which a rich cluster is formed at the center of a simulation sphere of radius 30 Mpc (Hoffman & Ribak 1991). The constraint that we impose is the 3σ peak with the 8 Mpc Gaussian smoothed density field at the center of the simulation sphere. To get enough resolution with a relatively small number of particles, we use the multimass initial condition for simulation B (Navarro, Frenk, & White 1996; Huss, Jain, & Steinmetz 1997). This initial condition is made as follows:

First, only long-wavelength components are used for the realization of initial perturbation in the simulation sphere using $\sim 10^5$ particles, and then we perform a simulation with these low-resolution particles. After this procedure, we tag the particles which are inside a sphere of radius 3 Mpc centered on the cluster center at $z = 0$. Next, we divide the tagged particles according to the density perturbation that is produced by additional shorter wavelength components. The mass of a high-resolution particle is 1/64 that of a low-resolution one. As a result, the total number of the particles becomes $\sim 10^6$. Our analyses are operated only for the high-resolution particles. The mass of a high-resolution particle is $m \simeq 10^9 M_\odot$, and its softening length, ϵ , is set to 5 kpc.

2.2. N-Body Calculation

To follow the motion of the particles, we use a tree code (Barnes & Hut 1986) with the angular accuracy parameter $\theta = 0.75$ radians, and we include quadrupole and octopole moments in the expansion of the gravitational field.

The numerical calculation is started from redshift $z = 20$, and it is integrated by using individual time steps (Hernquist & Katz 1989). A time step for particle i is given as

$$\Delta t_i = C \left(\frac{\epsilon^2}{a_i} \right)^{1/2}, \quad (1)$$

where C is a constant and a_i is the acceleration of particle i . This constant, C , is set to 0.25. In this case, errors in total energy are less than 1% through our simulations.

2.3. Halo Identification

Finding galactic halos in dense environments is challenging work. The most widely used halo-finding algorithm, called the friends-of-friends algorithm (e.g., Davis et al. 1985), and the spherical overdensity algorithm (Cole & Lacey 1994; Navarro, Frenk, & White 1996) are not acceptable (Bertschinger & Gelb 1991), because they cannot separate substructures within large halos.

The DENMAX algorithm (Bertschinger & Gelb 1991; Gelb & Bertschinger 1994) makes significant progress but requires a substantial amount of CPU time in actual calculations. Since we often search halos through our simulations, we adopt lighter numerical procedures with good performance. Therefore, we use the adaptive friends-of-friends algorithm (Suto, Cen, & Ostriker 1992; Sugino & Suto 1992; van Kampen 1995), which enables us to avoid the problem in the friends-of-friends algorithm by using local densities to determine local linking lengths. Moreover, we remove unbound particles from halos found by this algorithm. This procedure is important for galactic halos in groups and clusters.

In our adaptive friends-of-friends algorithm, a local linking length, b_{ij} , is calculated as follows:

$$b_{ij} = \beta \min \left[L_p, \frac{\rho_i(r_s)^{-1/3} + \rho_j(r_s)^{-1/3}}{2} \right], \quad (2)$$

where

$$\rho_i(r_s) = \frac{1}{(2\pi r_s^2)^{3/2}} \sum_{j=1}^N \exp \left(-\frac{|\mathbf{r}_i - \mathbf{r}_j|^2}{2r_s^2} \right), \quad (3)$$

L_p is the mean particle separation, r_s is the filtering length to obtain a smoothed density field, and \mathbf{r}_i is the position of the particle i . We specify a combination of the value of two parameters, β and r_s , in our algorithm as follows. For β we require that our algorithm be equivalent to the conventional friends-of-friends algorithm in the field region, so β is set to 0.2, which corresponds to the mean separation of particles in a virialized object. The filtering length, r_s , should be determined depending on the size of objects in which we are interested. Thus, it must be larger than the size of galactic halos and smaller than the size of clusters. In this paper we set it to 1 Mpc after several tests.

TABLE 1
PARAMETERS OF TWO SIMULATIONS^a

Simulation	Constraint	N_h	N_l	ϵ_h (kpc)	ϵ_l (kpc)	m_h (M_\odot)	m_l (M_\odot)	Size (Mpc)	M_{most} (M_\odot)
A	None	91911	...	5	...	1.08×10^9	...	7	1.6×10^{13}
B	3σ peak	958592	97953	5	50	1.08×10^9	6.9×10^{10}	30	9.3×10^{14}

^a Subscripts h and l indicate high-resolution and low-resolution particles, respectively.

After identifying galactic halos, we remove the unbound particles. At first we compute the potential, ϕ_i , for each particle i due to all members of the halo:

$$\phi_i = \sum_{j \neq i}^{N_h} \phi(r_{ij}), \quad (4)$$

where N_h is the number of particles belonging to the halo. We then iteratively remove unbound particles as follows. We compute the energy $E_i = \frac{1}{2}m|\mathbf{v}_i - \mathbf{v}_h|^2 + \phi_i$ for each particle in the halo, where \mathbf{v}_h is the mean velocity of the member particles. We then remove all particles with $E_i > 0$. The procedure is repeated until no more particles are removed. Finally, it is identified as a galactic halo when it contains more particles than the threshold number, n_{th} , which is usually set to 15 in this paper. We show some tests on our halo-finding algorithm in § 3.1.

2.4. Creation of Merging History Trees of Galaxies

Our method of creating galaxy merging history trees resembles the method that was used by Summers et al. (1995). The main improvement is that we trace “halo stripped galaxies” as well as galactic halos because halo disruption is probably due to insufficient resolution (Moore et al. 1996a) and lack of dissipative processes (Summers et al. 1995).

To follow the evolution of galaxies in our simulation, we identify the galactic halos at 26 time stages with a 0.5 Gyr time interval. The three most bound particles in each galactic halo are tagged as tracers. We consider three cases to follow their merging histories. First, for a galactic halo at a time stage t_{i+1} , where i is the number of a time stage, if the halo has more than two tracers that were contained in the same halo at the previous time stage, t_i , then the halo at t_{i+1} is a “next halo” of the halo at t_i . In this case, the halo at t_i is an “ancestor” of the halo at t_{i+1} .

Next, we consider the case that some halos at t_{i+1} have one of three tracers of a halo at t_i , the halo which has the tracer that was more bound in the halo at t_i is defined as the “next halo” of the halo at t_i .

We now consider the final case. When none of three tracers of a halo at t_i are contained in any halos at the next time stage (t_{i+1}), we define the most bound particle in this halo at t_i as a “stripped tracer.” Then we call both of the halos and the stripped tracers the “galaxies” throughout this paper.

In this way, we construct merging history trees of galaxies. In order to estimate the mass of a stellar component of a galaxy, we assume that the mass of the stellar component is proportional to the sum of the masses of its all “ancestors” (hereafter we call this mass the “summed-up mass”). Except for the case in which a large fraction of the stellar component of the galaxy was stripped during the halo stripping, this assumption may be valid. To consider mass increase due to accretion of dark matter to the halo after its first identification, we replace the summed-up mass with the halo mass when the summed-up mass is smaller than the halo mass.

The reason for using three tracers for each halo is to avoid the possibility that we may select an irregular tracer that happens to appear near the density peak of the halo. However, for almost all halos we get the same result even if we use a single tracer for each halo. Therefore, three tracers are enough to avoid this possibility.

3. RESULTS

3.1. Galactic Halos in N-Body Simulation

In this subsection we show the results of some tests of our halo-finding algorithm to show its features and to check its reliability.

First, we present the distribution of dark matter and halos in the simulated cluster at $z = 0$ in Figure 1. The upper panel is an x - y projection of a density map in a cube with sides $2r_{200}$ (r_{200} is the radius of the sphere having overdensity $\delta = 200$) centered on the cluster. The gray scale represents logarithmic scaled density given by the smoothed particle hydrodynamics (SPH)-like method with neighboring 64 particles (Hernquist & Katz 1989). The x - y projection of the particles contained in galactic halos identified by our halo-finding algorithm is plotted in the lower panel in Figure 1. It is found from Figure 1 that many galaxy size density peaks survive even in the central part of the rich cluster, and our halo-finding algorithm can pick up these peaks as halos.

Next, we compare the density profiles of the halos in simulation A (hereafter we refer them to field halos) with the density profile proposed by Navarro, Frenk, & White (1996, hereafter NFW).

The NFW profile approximates profiles of virialized objects obtained by cosmological N -body simulations well, and it is written as follows:

$$\rho(r) = \frac{\rho_c \delta_c}{(r/r_s)(r/r_s + 1)^2}, \quad (5)$$

where ρ_c is the critical density of the universe,

$$\delta_c = \frac{200}{3} \frac{c^3}{\ln(1+c) - c/(1+c)}, \quad (6)$$

and

$$r_s = r_{200}/c, \quad (7)$$

and r_{200} is a radius of a sphere whose mean density is 200 times as large as the mean density of the universe. In Figure 2 we plot the density profiles of the field halos obtained by our halo-finding algorithm (plus signs), the profiles based on the spherical overdensity algorithm for $\delta = 200$ (crosses), and the NFW fits for latter profiles (solid lines). We find that the halos identified by our halo-finding algorithm are well fitted by the NFW model except for very massive ones, and these massive halos have smaller radii than r_{200} because it separates the dominant halos and their companions. It is also found that these halos have cores and their sizes are comparable to the softening length, ϵ , potential. These cores are numerical artifacts due to the softened potential and they make it easier to disrupt these halos by tidal force.

As we mentioned above, our method can pick up galaxy size density peaks even in the cluster environment, and most selected halos without substructures in the field show the NFW profiles. However, since this method is improved only to avoid the clouds-in-clouds problem, we should use an alternative independent method for cluster halos when we argue their radii and outer density profiles.

We can define the radius of a halo within the cluster using the halo density profile $\rho(r)$, where r is the distance from the center of the halo, and measuring the radius at which $\rho(r)$ flattens due to dominance of the cluster background density (Klypin, Gottlöber, & Kravtsov 1997; Ghigna et al. 1998). At the radius where the density profile is flattened, the

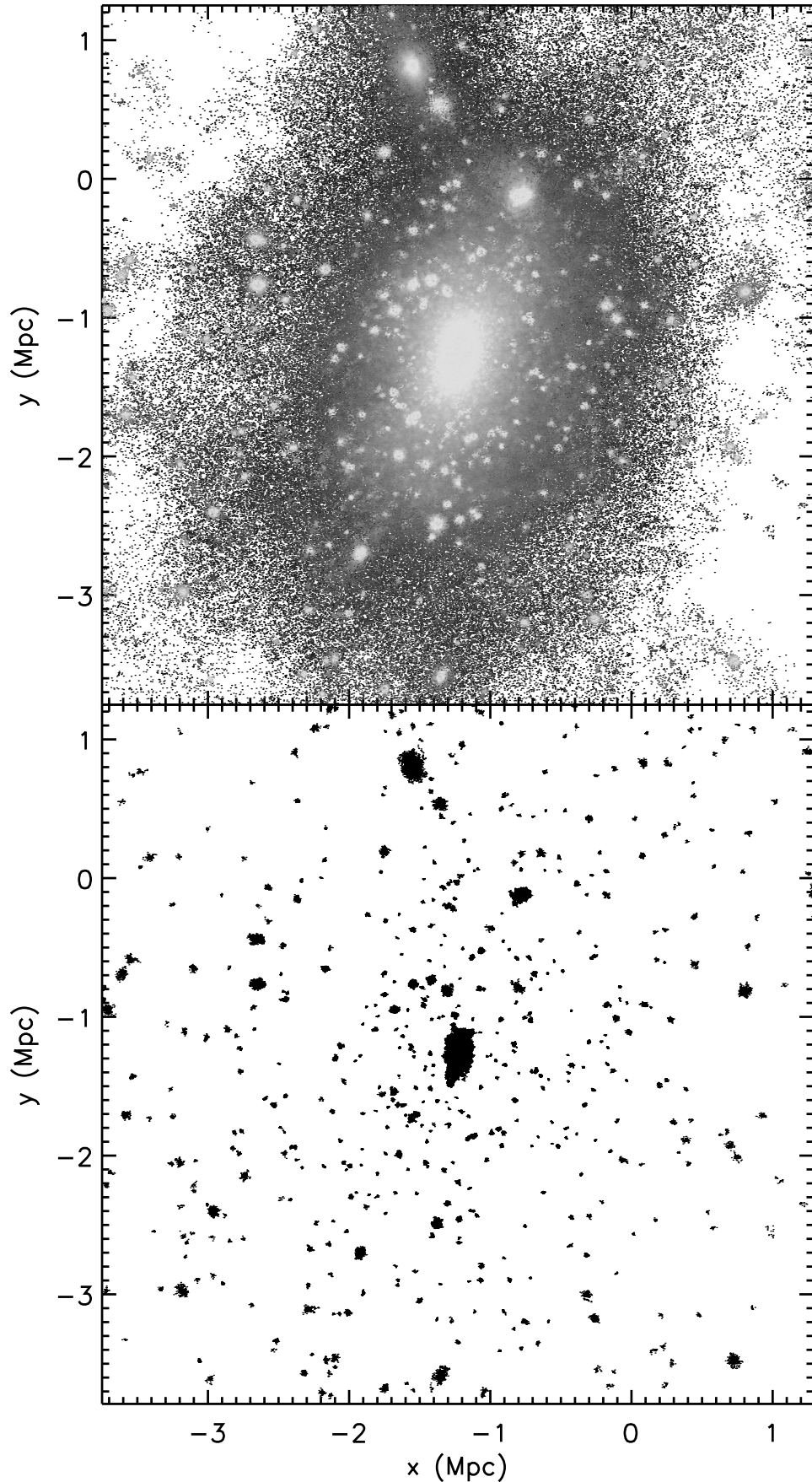


FIG. 1.—Density map (*upper panel*) and the x - y projection of the particles contained in the galactic halos (*lower panel*) within the cluster's virial radius at $z = 0$.

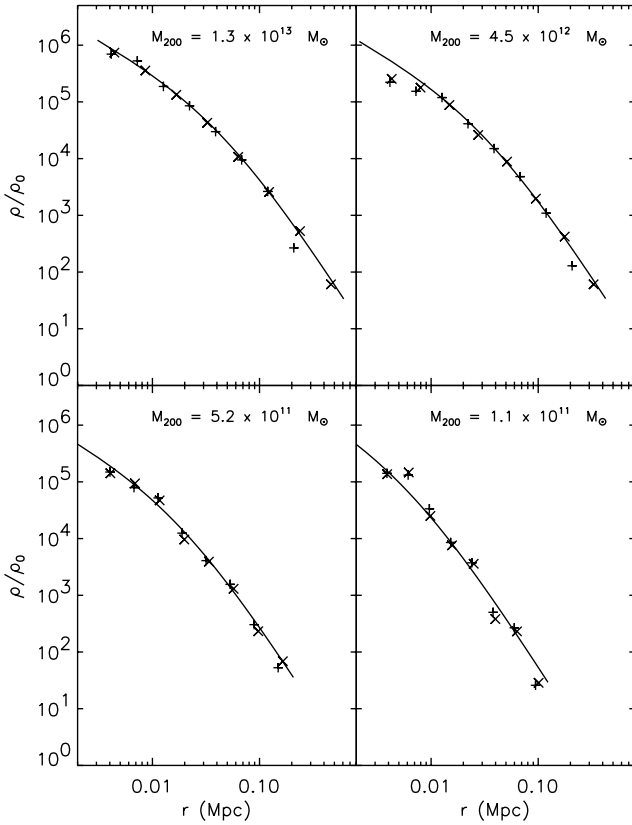


FIG. 2.—Density profiles of field halos. Plus signs and crosses represent the density profiles obtained by our halo-finding algorithm and the spherical overdensity algorithm, respectively. Solid lines represent the NFW fits for the profiles by the spherical overdensity algorithm.

profile of the circular velocity, $v_c = [GM(r)/r]^{1/2}$, turns around and increases (Ghigna et al. 1998). The radius where $\rho(r)$ flattens and that where v_c takes a minimum value are essentially equal (see Fig. 3). Therefore, we refer to the radius at which v_c takes a minimum value as the radius of a cluster halo. It should be noted that this method allows overlap of halos, that is, if we estimate the mass of a halo by this method, the mass of a halo includes the mass of the satellite's halos. Therefore, we cannot determine the mass of a halo by the v_c method.

Our halo finding algorithm seems to underestimate the extent of the cluster halo comparing with that obtained by the v_c method. Does this feature cause serious problems in estimating the summed-up mass of galaxies? Before cluster-size objects form, we can estimate their size correctly, because such an environment is similar to the field environment, and our finding algorithm gives reasonable halos in the field (Fig. 2). After the objects fall into the cluster, there are three ways to increase their summed-up mass, that is, merging with other halos, merging with stripped tracers, and accretion of dark matter particles. Since our method identifies halos according to density peaks, we can treat merging of halos (i.e., peaks) properly independent of their size. Only when stripped tracers are near enough to a density peak of a halo, should this be regarded as merging; therefore underestimation of the extent of halos may not matter. When cluster halos increase their mass by accretion of dark matter, we cannot estimate the increase of their summed-up mass properly; however, such cases may be rare, because the size of halos is diminished by tidal inter-

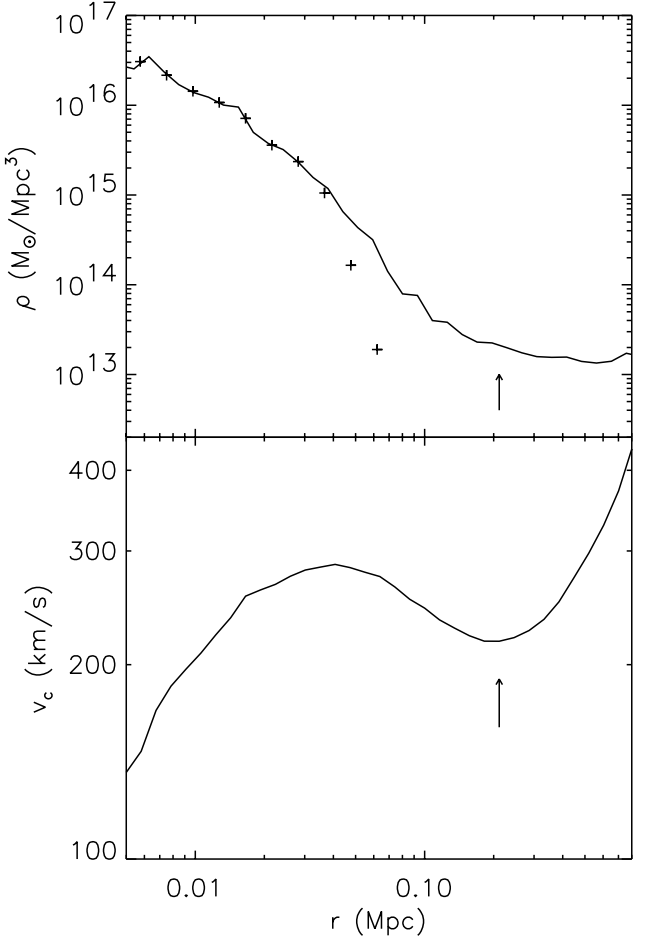


FIG. 3.—Density profile (upper panel) and circular velocity profile (lower panel) of a galactic halo in the cluster at $z = 0$. The density profile obtained by our halo-finding algorithm is represented by plus signs. The radius of the halo obtained by the v_c method is indicated by upward-pointing arrows.

actions in the cluster, as we will show in § 3.4.3. Thus, we conclude that we can estimate the summed-up mass of the cluster halos by our method.

3.2. Evolution of the Whole Cluster

We define a sphere having a mean overdensity 200 as a virialized object, and we show mass, M_{200} , and radius, r_{200} , of the most massive virialized object at each time stage in simulation B in Table 2. It is found that a cluster-size object begins to form from redshift $z \simeq 1$; therefore we call this object a “cluster” after $z \simeq 1$. Indeed, the main clump of the cluster has already formed at $z = 1$ and it does not undergo major merging after $z = 1$ (Fig. 4). We define the formation redshift, z_{form} , of the final cluster (cluster at $z = 0$) as the redshift when it has accreted half of its final mass (Lacey & Cole 1993); thus its formation epoch is $z_{\text{form}} \sim 0.15$ (see Table 2).

The density profiles and the velocity dispersion profiles of the cluster are shown in Figures 5 and 6, respectively. The distribution of the dark matter inside r_{200} changes little with time (see thin lines in the upper panels of Figs. 5 and 6). It agrees with the fact that this cluster evolves mainly by the accretion of dark matter and small clumps (Fig. 4). The density profile at $z = 0$ (thin solid line) is well fitted by the NFW model (thick solid line), except for the central cusp ($r < 100$ kpc) where its slope [$\rho_{\text{cusp}}(r) \propto r^{-1.35}$] is steeper

TABLE 2

MASS OF MOST MASSIVE VIRIALIZED OBJECT
 M_{200} AND ITS RADIUS r_{200} AT
 EACH TIME STAGE

t (Gyr)	Redshift	r_{200} (Mpc)	M_{200} (M_\odot)
0.5	7.4	0.04	4.4×10^8
1.0	4.4	0.10	1.1×10^{10}
1.5	3.2	0.17	6.8×10^{10}
2.0	2.4	0.30	4.5×10^{11}
2.5	2.0	0.39	1.2×10^{12}
3.0	1.6	0.51	2.9×10^{12}
3.5	1.4	0.60	5.2×10^{12}
4.0	1.2	0.72	9.9×10^{12}
4.5	1.0	0.87	1.9×10^{13}
5.0	0.89	1.02	3.4×10^{13}
5.5	0.77	1.21	5.8×10^{13}
6.0	0.67	1.32	8.0×10^{13}
6.5	0.58	1.42	1.0×10^{14}
7.0	0.51	1.51	1.3×10^{14}
7.5	0.44	1.58	1.6×10^{14}
8.0	0.38	1.68	2.0×10^{14}
8.5	0.33	1.77	2.4×10^{14}
9.0	0.28	1.85	2.9×10^{14}
9.5	0.23	1.94	3.4×10^{14}
10.0	0.19	2.03	4.1×10^{14}
10.5	0.15	2.13	4.8×10^{14}
11.0	0.12	2.21	5.6×10^{14}
11.5	0.08	2.31	6.6×10^{14}
12.0	0.05	2.38	7.4×10^{14}
12.5	0.03	2.45	8.3×10^{14}
13.0	0.0	2.52	9.3×10^{14}

than the NFW profile [$\rho_{\text{cusp}}(r) \propto r^{-1}$] and is well consistent with that obtained by Moore et al. (1998a), who give $\rho_{\text{cusp}}(r) \propto r^{-1.4}$. In our case, the softening length, $\epsilon = 5$ kpc, is much smaller than $r_s = 300$ kpc, and, moreover, the number of particles that are inside the virial radius of the cluster is about 2 orders of magnitude larger than that of the NFW simulation. Thus, we conclude that we have enough resolution to argue for a density profile of central cusp (20 kpc $< r < 100$ kpc).

The number density profiles of halos in the cluster are plotted in the lower panel of Figure 5 (thin lines). The number density of the halos decreases with time, especially in the central part of the cluster. The thick solid line and the thick dashed line denote the dark matter density, ρ_d , and the number density of galaxies which consist of both halos and stripped tracers and these values are normalized by the values at r_{200} , respectively. We can see that the halo distribution is “antibias” with respect to the dark matter distribution. It is because a softened halo has a core with $r_{\text{core}} \sim \epsilon$, therefore, it is rapidly disrupted by the encounters with other halos and the tidal field of the cluster when $r_{\text{tidal}} < (3-4)\epsilon$ (Moore et al. 1998b). This scale is small enough for large halos ($M_h > 10^{11} M_\odot$); thus when such halos are disrupted, we can say that they are stripped significantly. Since such disruption is an artificial numerical effect and is due to lack of physics (i.e., lack of dissipational effects), we expect that if we perform simulations with infinite resolution or with baryonic components, the number density of galaxies is similar to that of the galaxies obtained here, which we get by assuming that no galaxy is disrupted completely. The number density of the galaxies at $z = 0$ (thick dashed line) shows no “bias” with respect to the dark

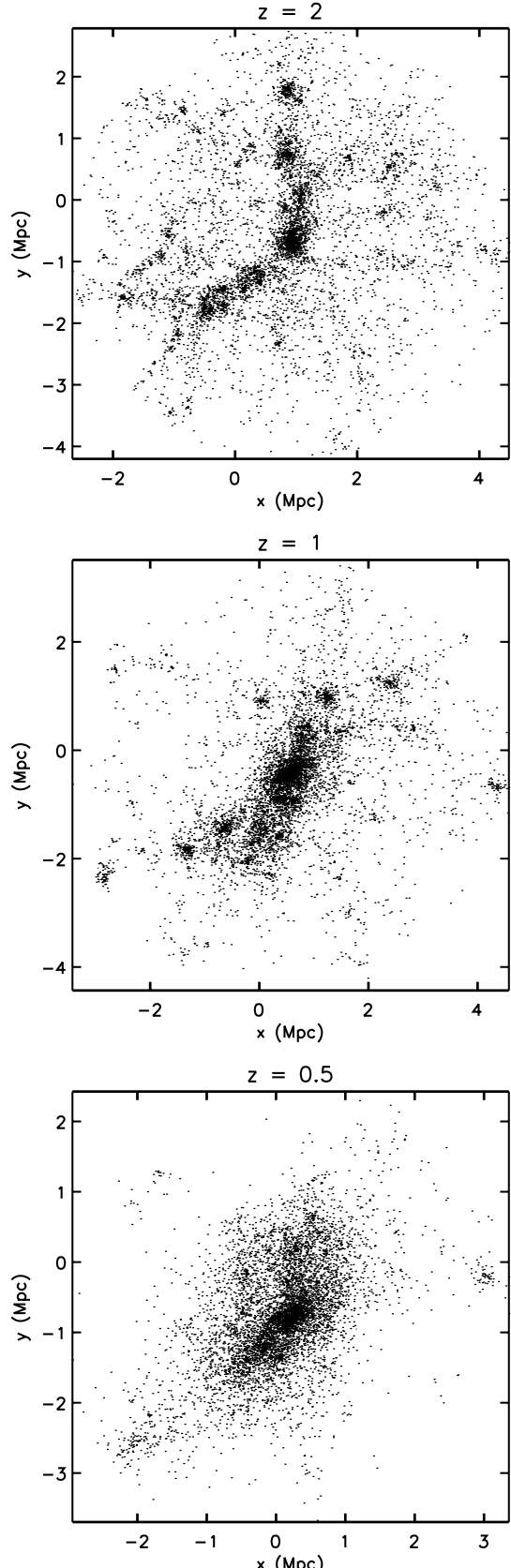


FIG. 4.—Particle plots illustrating the time evolution of the cluster. One percent of the particles that are placed in the sphere having the same mass as the final cluster are plotted.

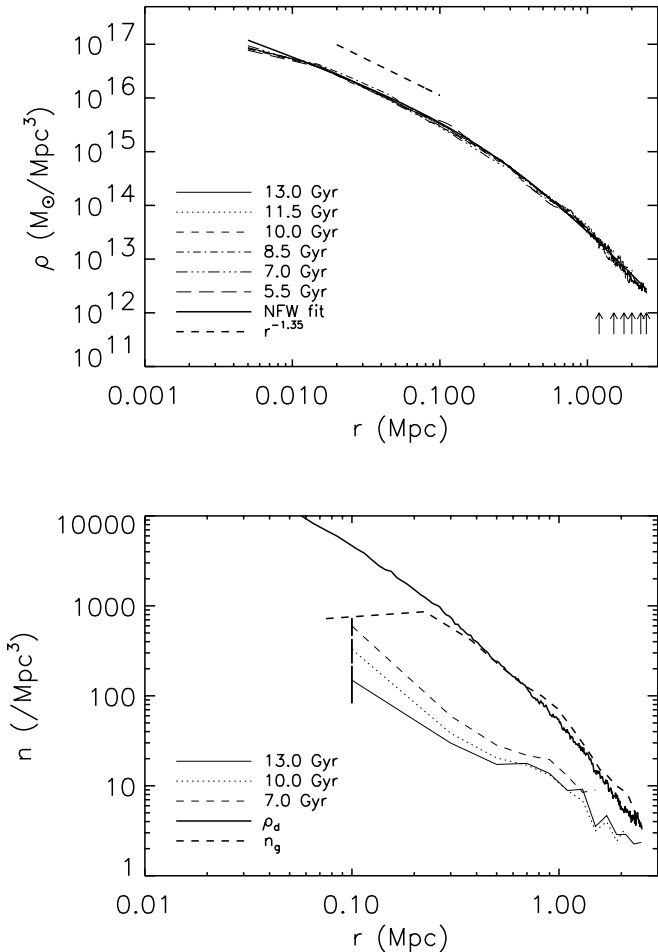


FIG. 5.—Density profiles (*upper panel*) and halo number density profiles (*lower panel*) of the cluster. The solid line in the upper panel is the NFW fit. The thick solid line and the thick dashed line in the lower panel represent dark matter and galaxy distribution at $z = 0$, respectively. Both are renormalized according to their values at r_{200} . The radii of the clusters, r_{200} , are indicated by upward-pointing arrows. The error bars are 1σ Poissonian uncertainties estimated from the number of halos in the first bin.

matter density except for the central part of the cluster, where a central massive halo dominates (Fig. 1). This result differs from that of van Kampen (1995), who suggested that galaxies are more concentrated than dark matter. We guess that their result was the artifact produced by the artificial cooling adopted in his model.

To show the effect of the dynamical friction and the domination of the central very massive halo, we plot the mass-weighted velocity dispersion of galactic halos in the lower panel of Figure 6. In the central part of the cluster, it has a smaller value than that of dark matter (*upper panel*). The difference between these two velocity dispersions implies that the large halos are slowed down by the dynamical friction, and a central massive halo becomes dominant in this region. Except for the central region, the velocity dispersion of the cluster halos is almost the same as that of the dark matter. Therefore, we cannot find the “velocity bias” which Carlberg (1994) has found for the simulated cluster galaxies.

The dark matter velocity dispersion profile also decreases from $r \simeq 200$ kpc toward the center. This is consistent with the fact that the density profile within this radius is shallower than the isothermal profile, $\rho(r) \propto r^2$. We make the

interpretation that the cold component in the central cusp of the cluster ($r < 200$ kpc) is due to the contribution of the low velocity dispersion dark matter component that is confined in the potential well of the central dominant halo, which is always placed at the center of the cluster. We will show some features of this halo in the next section.

3.3. Evolution of the Central Dominant Halo

In simulation B, the most massive halo is always seen at the center of the cluster; thus we call this halo the “central dominant halo” (CDH). There is no doubt about the existence of the CDH in our simulated cluster, because 75% of the particles that were identified as members of the CDH at $z \simeq 0.5$ also remain in the CDH at $z = 0$. The remaining 25% of them probably belong to the cluster.

The mass evolution of the CDH that is identified by our halo-finding algorithm is presented in Figure 7. The mass of the CDH increases quickly from $z \simeq 0.4$. It always absorbs 15–30 galaxies of the former time stage. Therefore, we can say that the CDH has evolved through merging and accretion. Aragón-Salamanca, Baugh, & Kauffmann (1998) estimated that the stellar mass component in the brightest cluster galaxies (BCGs) have grown by a factor of 4–5 for critical density models from $z \simeq 1$ by using the observed magnitude-redshift relation of the BCGs and evolutionary population synthesis models. The trend of the increase of mass of the CDH seems to be consistent with their result

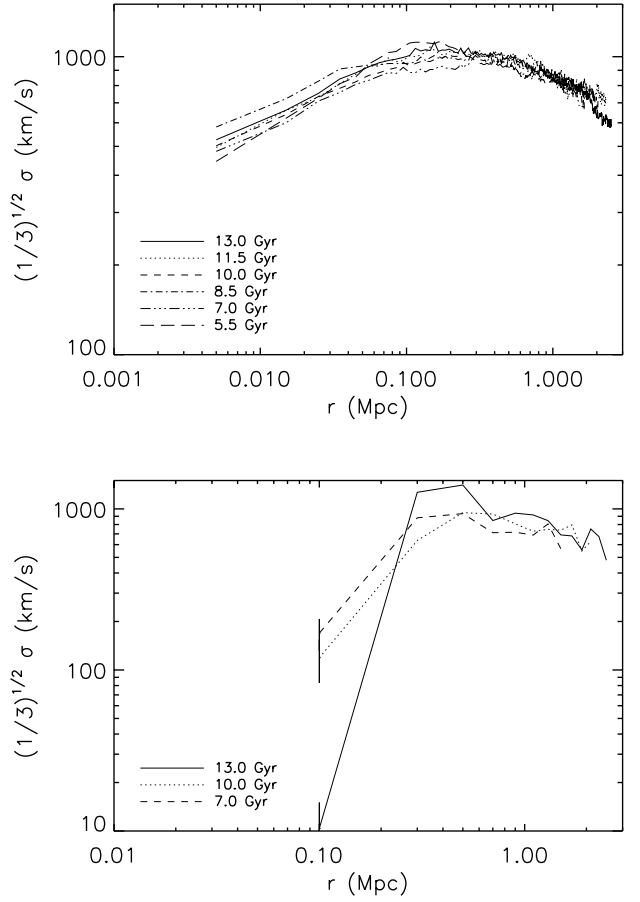


FIG. 6.—Dark matter velocity dispersion profiles (*upper panel*) and the mass-weighted halo velocity dispersion profiles (*lower panel*) of the cluster. The error bars are 1σ Poissonian uncertainties estimated from the number of halos in the first bin.

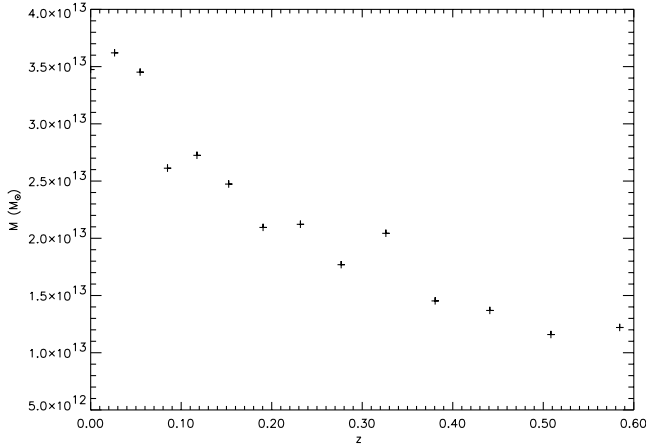


FIG. 7.—Growth of the central dominant halo of the cluster with redshift z .

and with the predictions by semianalytic models (Kauffmann et al. 1993; Cole et al. 1994; Aragón-Salamanca et al. 1998). However, since there is ambiguity in distinguishing the component of the CDH from that of the cluster and it is difficult to determine the extent of the CDH in our dissipationless simulation, we should perform simulations including hydrodynamic processes to investigate the evolution of the CDH and the stellar component within the CDH realistically, and that is left for further studies.

3.4. Formation and Evolution of the Galactic Halos in the Cluster

3.4.1. Mass Functions

It is interesting to compare the mass function of galaxies in a region which becomes the final cluster in simulation B (hereafter the “precluster” region) to that of simulation A (hereafter the “field” region) before larger objects (groups and clusters) have formed. In the field region, since effects of tidal stripping are negligible, stripped tracers are rare objects, and the summed-up mass function of galaxies and the mass function of halos are almost the same. Figure 8 shows that the summed-up mass functions in both regions at $z = 2$ are very similar except for the existence of very massive galaxies ($m_{\text{sum}} \gtrsim 10^{12} M_{\odot}$) in the precluster region. The absence of high-mass galaxies in the field region may be a consequence of the small volume of simulation A. However, it is also likely that this difference is naturally explained by the peak formalism (Bardeen et al. 1986), which predicts that rare peaks at a mass scale that we selected as the massive halos should be highly correlated in space, that is, they are likely to form in high-density regions at a larger mass scale.

It is also interesting to compare the above mass functions to the mass function expected from the Press-Schechter (PS) formalism (Press & Schechter 1974; Lacey & Cole 1993) and the conditional mass function (Lacey & Cole 1993). By the PS formula (here in the notation of Lacey & Cole), the number density of halos with mass between M and $M + dM$ at z is

$$\frac{dn}{dM} (M, t) dM = \frac{\rho_0}{M} f(S, \omega) \left| \frac{dS}{dM} \right| dM , \quad (8)$$

where

$$f(S, \omega) dS = \frac{\omega}{(2\pi)^{1/2} S^{3/2}} \exp \left(-\frac{\omega^2}{2S} \right) dS , \quad (9)$$

$S = \sigma(M)^2$ is the variance of the linear density field of mass scale M , and $\omega = \delta_{\text{th}}(1 + z)$ is the linearly extrapolated threshold for the density contrast required for structure formation.

The conditional mass function, that is, the number of halos with mass between M_1 and $M_1 + dM_1$ at z_1 that are in a halo with mass M_0 at z_0 ($M_1 < M_0$, $z_0 < z_1$) is:

$$\begin{aligned} \frac{dN}{dM_1} (M_1, z_1 | M_0, z_0) dM_1 &= \frac{M_0}{M_1} f(S_1, \omega_1 | S_0, \omega_0) \\ &\times \left| \frac{dS}{dM} \right| dM_1 , \end{aligned} \quad (10)$$

where

$$\begin{aligned} f(S_1, \omega_1 | S_0, \omega_0) dS_1 &= \frac{\omega_1 - \omega_0}{(2\pi)^{1/2} (S_1 - S_0)^{3/2}} \\ &\times \exp \left[-\frac{(\omega_1 - \omega_0)^2}{2(S_1 - S_0)} \right] dS_1 . \end{aligned} \quad (11)$$

In Figure 9 we plot equation (8) with $\delta_{\text{th}} = 1.69$, assuming spherical collapse for the density contrast (Lacey & Cole 1993), and equation (10) with $z_1 = 2$, $z_0 = 0$, and $M_0 = M_{200}(z = 0)$. In this mass range, there is not so much difference between the PS mass function and the conditional mass function, and the summed-up mass function in both regions shows good agreement with the PS mass function at $z = 2$. The reason why the summed-up mass function in the precluster region agrees better with the PS mass function than with the conditional mass function in the high-mass range may be that our halo-finding algorithm divides a large halo into small halos according to density peaks; thus, if we use the friends-of-friends or the spherical overdensity algorithm, this mass function may be more similar to the conditional mass function.

To investigate the effects of cluster formation on the cluster galaxies, we plot the summed-up mass function in the cluster at $z = 0$ in Figure 9. Although the summed-up mass function of field galaxies evolves similar to the PS theory, that of the cluster galaxies hardly evolves from $z = 2$ except for the existence of several very massive galaxies. This result implies that most of cluster galaxies have not increased their mass of the stellar component very much by merging and accretion from $z \simeq 2$.

These features seem to be consistent with the observed old population of cluster ellipticals, that is, the bulk of their stellar population was formed at $z > 2$ and then passively evolved until the present day (Ellis et al. 1997), estimated from the surprisingly tight color-magnitude relation both at present (Bower, Lucey, & Ellis 1992) and at higher z (Ellis et al. 1997). However, inclusion of star formation processes and gasdynamics in our models is needed for more detailed investigation of the color-magnitude relation and the ages of cluster galaxies.

3.4.2. Merging of Galaxies

A halo that has more than two ancestors at the former time stage is defined as a “merger remnant.” In Figure 10

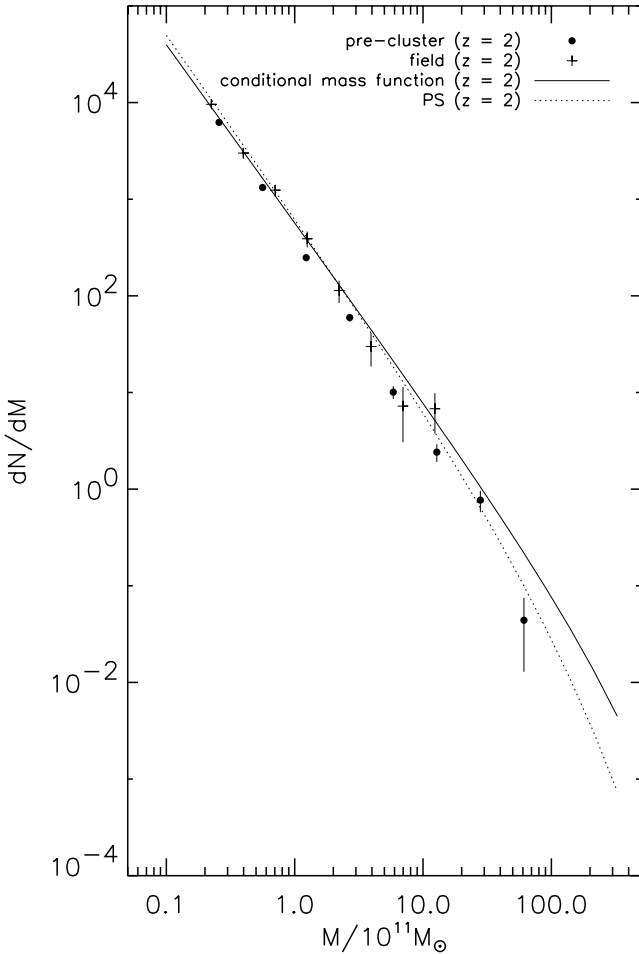


FIG. 8.—Summed-up mass functions in the precluster region (filled circles) and in the field region (plus signs) at $z = 2$; the error bars are 1σ Poissonian uncertainties estimated from the numbers of galaxies in each mass bin. The solid line indicates the conditional mass function at $z = 2$ with $z_0 = 0$ and $M_0 = M_{200}(z = 0)$, and the dotted line indicates the PS mass function. The mass function in the field region and the PS mass function are renormalized to indicate the number of galaxies in mass M_0 .

we show the merger remnant fraction of the large galaxies ($M_{\text{sum}} \geq 10^{11} M_\odot$) as a function of redshift. In counting the number of merger remnants, we include the galaxies that have undergone minor mergers as well as major mergers because minor mergers also can lead to starbursts (Hernquist 1989). We find that this fraction in the region dominated by the high-resolution particles in simulation B (hereafter the “cluster-forming” region) is larger than that in the field at high redshift ($z \gtrsim 3$), as expected from analytic work (Bardeen et al. 1986; Kauffmann 1996), that is, for a random Gaussian field, redshifts of collapse of galaxy scale density peaks are boosted by the presence of surrounding, large-scale overdensity. Therefore, the presence of larger objects at $z \simeq 2$ in the cluster formation region than in the field (see Fig. 8) is well explained by the difference of merging efficiency between in the cluster formation environment and in the field. On the other hand, it is also found that after $z \sim 3$ this fraction in the cluster-forming region decreases rapidly and becomes smaller than that in the field, and this fraction is always less than 10% inside the cluster’s virial radius. This decline of the merger remnant fraction of cluster galaxies is due to high velocity dispersion of the larger objects, that is, if the relative velocity of a pair of

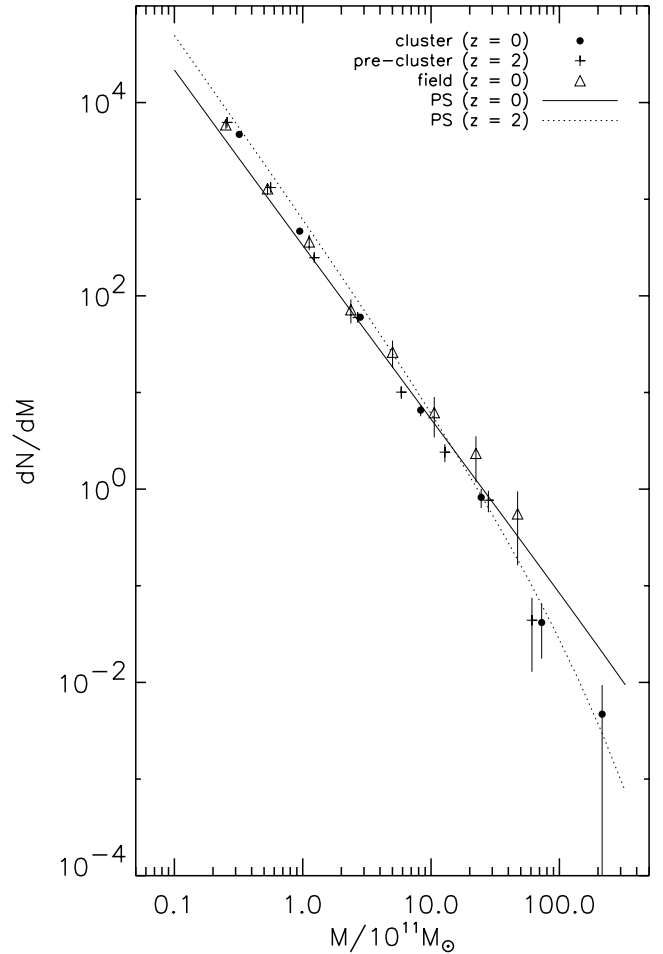


FIG. 9.—Summed-up mass function of galaxies in the cluster (filled circle) at $z = 0$. The summed-up mass function in the precluster region at $z = 2$ (plus signs) and one in the field region at $z = 0$ (triangles) are also plotted. The solid line and the dotted line indicate the PS mass functions at $z = 0$ and $z = 2$, respectively.

galaxies is larger than the inner velocity dispersion of the halos of these galaxies, they cannot merge (Binney & Tremaine 1987). Moreover, the stripping of halos by tidal fields of the groups and clusters also prevents merging of individual halos (Funato, Makino, & Ebisuzaki 1993; Bode et al. 1994). Clearly, this decrease is the reason why the summed-up mass of cluster galaxies has not evolved after $z \simeq 2$.

Because the large halos preferentially merge, about 30% of the cluster galaxies with $M_{\text{sum}} > 10^{11} M_\odot$ at $z = 0$ have undergone merging since $z \simeq 0.5$, while only 8% of all the cluster galaxies have undergone it since $z \simeq 0.5$.

3.4.3. Tidal Stripping of Halos

To show the effect of tidal stripping on the galactic halos, we investigate whether large halos ($M_h \geq 10^{11} M_\odot$) at high redshift ($z \simeq 2$) are found as halos at lower redshift. Unless their descendants become stripped tracers for $n_{\text{th}} = 10$, we call their descendants “surviving halos.” If their descendants become stripped tracers, it means that they have lost a large fraction of their original halo mass, and in this case dissipative effects, which are not included in our simulation, should become important. In Figure 11 we show the surviving fraction and the stripped fraction of such galaxies in the 0.5 Mpc radius bins from the cluster center. At $z \simeq 0.5$, a

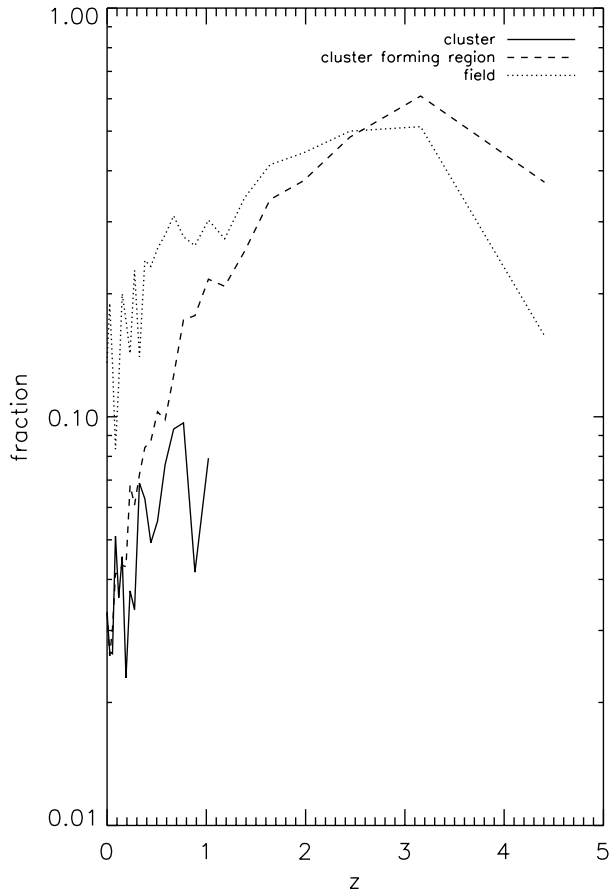


FIG. 10.—Merger remnant fractions of the massive galaxies with $M_{\text{sum}} > 10^{11} M_{\odot}$ in the cluster (solid line), in the cluster-forming region (Ie), and in the field (dotted line).

large fraction of halos (60%–100%) has survived (*upper panel*). On the other hand, at $z = 0$ (*lower panel*), more than 60% of the halos have been destroyed in the central part of the cluster, and these fractions have a clear correlation with the distance from the cluster center. Although we may have overestimated the stripping effect due to the softened potential for each particle (Moore et al. 1996a), lack of dissipative effects (Summers et al. 1995), and the feature of our halo-finding algorithm (see § 3.1), we expect that these stripped galaxies are actually stripped significantly, because two former effects appear only at a very small scale ($r \lesssim 3\epsilon$); our halo-finding algorithm can pick up very small density peaks within the cluster, and we treat only large halos here.

Recently, Ghigna et al. (1998) have independently presented results similar to ours. However, they have shown only the evolution of the cluster halos from $z \simeq 0.5$. Clearly, the tidal stripping from the halo formation epoch is more important for the evolution of the galaxies. Our result shows that a number of cluster galaxies have already been strongly stripped of their halos at $z \simeq 0.5$.

Next we compare the radii of the halos, r_h , determined by the v_c method to the tidal radii of the halos estimated by the density of the cluster at their pericentric positions, r_{peri} , which we calculate by the NFW fit of the cluster density profile at $z = 0$. The mean ratio of pericentric to apocentric radii, $r_{\text{peri}}/r_{\text{apo}}$, is 0.2, and 26% of the cluster halos are on very radial orbits, $r_{\text{peri}}/r_{\text{apo}} < 0.1$. In spite of the difference in mass of the clusters, these values agree completely with

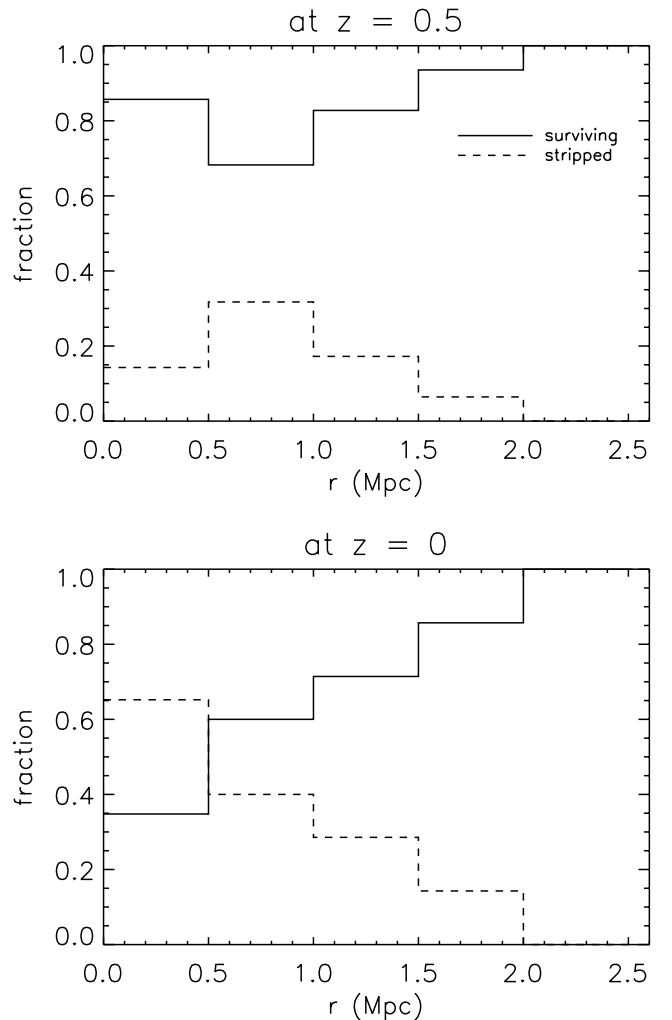


FIG. 11.—Surviving fraction (solid line) and stripped fraction (dashed line) of galaxies that have massive halos ($M_h > 10^{11} M_{\odot}$) at $z \simeq 2$. They are plotted in the 0.5 Mpc bins from the center of the cluster at $z \simeq 0.5$ (*upper panel*) and at $z = 0$ (*lower panel*).

those of Ghigna et al. (1998). The tidal radii of the halos, r_{est} , are estimated by the following approximation:

$$r_{\text{est}} \simeq r_{\text{peri}} \frac{v_{\text{max}}}{V_c}, \quad (12)$$

where v_{max} is the maximum value of the circular velocity of a halo and V_c is the circular velocity of the cluster. In Figure 12 we plot r_{est} against r_h for our outgoing halos that must have passed pericenter recently. We find that most of our halos have larger radii than r_{est} . Therefore, r_{est} seems to give roughly the minimum radius of a cluster halo. It is implied that the most dominant process that leads the mass loss of the large cluster halos is not the high-speed encounters with other halos but tidal stripping due to the global tidal field of the cluster, because galaxies should have smaller r_h if the high-speed encounters are important to mass loss of the cluster halos.

There is a difference between our result and the result of Ghigna et al. (1998), whose r_h shows much better agreement with r_{est} except for the halos with $r_{\text{peri}} < 300$ kpc, which have tidal tails due to impulsive collisions as they pass close to the cluster center.

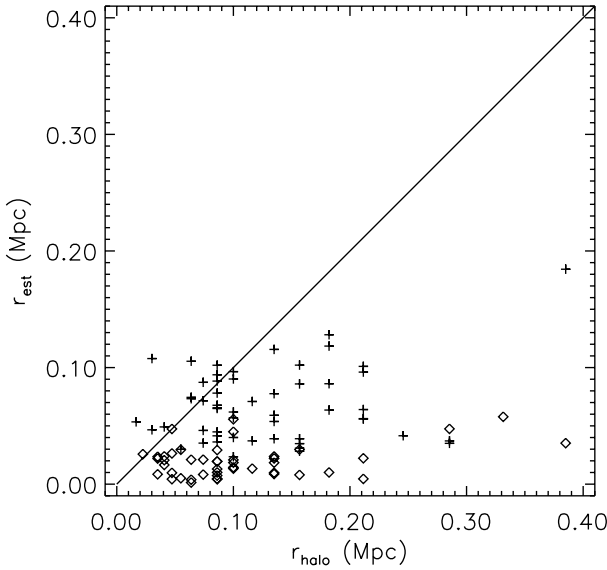


FIG. 12.—Measured values of halo tidal radii against their expected values, assuming that the halos have isothermal mass distributions that are tidally stripped at their pericentric positions. The plus signs represent outgoing halos (at $z = 0$). Diamonds denote those with $r_{\text{peri}} < 300$ kpc.

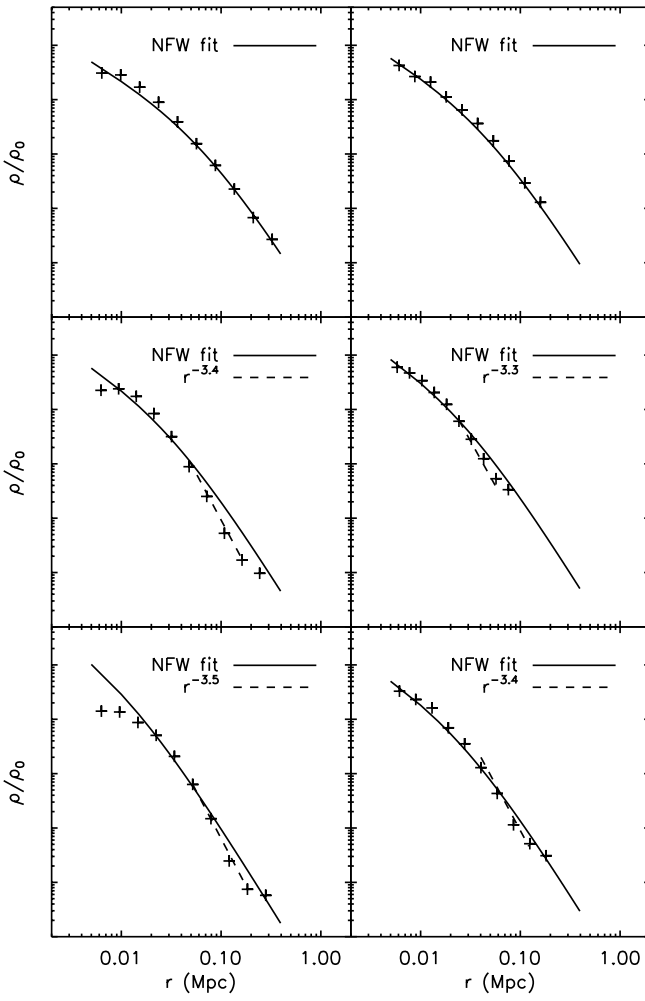


FIG. 13.—Comparison between the density profiles (at $z = 0$) of cluster halos (plus signs) and their fits by the NFW profiles (solid lines). The top row resents profiles of two massive halos with $r_{\text{peri}} > 500$ kpc and $r_h > 2r_{\text{est}}$. For other plots we show power-law fits for outer profiles of the halos (dashed lines) with $r_h \sim r_{\text{est}}$.

In our result, a number of our halos with $r_{\text{peri}} > 300$ kpc also have larger r_h than r_{est} .

We note that halos are not stripped instantly. The tidal stripping timescale, t_{st} , is roughly estimated as follows:

$$\frac{r}{R} \sim \left| \frac{d\Omega(R)}{dR} \right| rt_{\text{st}} ; \quad (13)$$

thus

$$t_{\text{st}} \sim \frac{3}{2} \frac{R}{V_c} , \quad (14)$$

where r is a radius of a halo, R is the distance from the center of the cluster, and $\Omega(R) = V_c(R)/R$ is an angular velocity at R . Using this formula, t_{st} is about 1 Gyr at $R \simeq 1$ Mpc. Our cluster has formed very recently ($z_{\text{form}} \sim 0.15$) because of its richness, that is, half of the cluster galaxies have accreted in the last 3 Gyr. Therefore, we conclude that the difference between our result and theirs is due to the difference in the formation epochs of the clusters, and our halos with $r_h > r_{\text{est}}$ have not yet been completely stripped.

It is interesting to compare the density profiles of the cluster halos and the NFW profile. To fit the density profiles of the cluster halos by equation (5), we also use r_{200} as a fitting parameter, because we do not obtain their r_{200} values from raw data. The top row of Figure 13 shows the density profiles of two halos [which are placed at $(-1.6, 0.8)$ and $(-0.8, -0.1)$, respectively, in Fig. 1] with $r_h > 2r_{\text{est}}$ and $r_{\text{peri}} > 500$ kpc. We expect that the effect of stripping may be small for such halos. For both halos, the NFW model can produce good fits. However, most of the halos that have $r_h \simeq r_{\text{est}}$ and $r_{\text{peri}} > 300$ kpc have steeper outer density profiles than the NFW model, as shown in the middle and bottom rows in Figure 13. Therefore, we can say that most of the halos are stripped in some degree and have steeper outer profiles, and some halos which have accreted recently to the cluster and which have not been stripped very much can retain their original shapes.

According to the NFW argument, the concentration parameter c in equation (5) should be higher for the cluster halos than for the field halos, because halos within denser

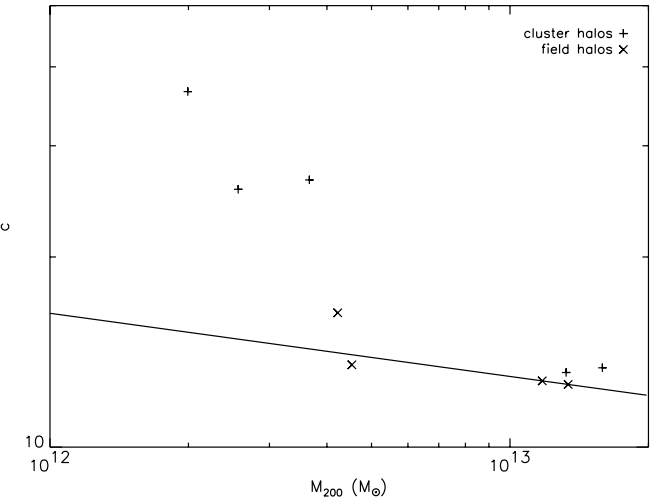


FIG. 14.—Concentration parameters for cluster halos (plus signs) and for field halos (crosses). The solid line denotes the analytic prediction by NFW.

environments form at earlier epochs. Since increasing the numerical resolution causes steeper inner profiles (Moore et al. 1998a), we choose the halos having resolution similar to those in the NFW simulation in both regions, and we plot the concentration parameter as a function of the M_{200} value for the halos in Figure 14. It is found that the field halos have almost the same values of the concentration parameter as those for the NFW theory (*solid line*), and the cluster halos are more concentrated than the field halos. Two cluster halos having values of c almost the same as the NFW theory values are halos that have recently undergone infall (Fig. 13, *top row*); thus, it is expected that they formed in a lower density region than other cluster halos. We should note that there is some ambiguity in determining the concentration parameters for cluster halos because they have steeper outer profiles due to tidal stripping than the NFW model, and this may lead to the higher value of c .

4. DISCUSSION

We investigate the formation and evolution of galaxy-size dark halos in a cluster environment based on the high-resolution N -body simulation. With our resolution (see Table 1) we find a number of galaxy size density peaks (about 300 with $n_{\text{th}} = 15$) within the virial radius of the cluster at $z = 0$. This result suggests that the overmerging problem can be much reduced by using high-resolution simulation. However, even with our resolution, a large number of halos cannot survive, even if they have massive halos at higher z . This makes it difficult to trace their merging histories, which play important roles when we investigate the evolution of cluster galaxies. To avoid this problem, we trace halo-stripped galaxies as well as galactic halos by using the particles placed at local density peaks of the halos as tracers. This approach enables us to derive merging history trees of galaxies directly from dissipationless N -body simulations in various kinds of environments.

We find the following results, which seem to relate to the evolution of the cluster galaxies, using this merging history tree:

1. The galaxy distribution in the cluster does not show either spatial or velocity bias except in the central part of the cluster, where the very massive halo dominates.

2. There is a very massive galactic halo at the center of the cluster, and a large fraction of dark matter particles in the central part of the cluster are confined in the local potential well of this halo. This halo has evolved through merging of the large halos and accretion of dark matter.

3. At $z \simeq 2$, the halo mass functions both in the field and in the cluster formation region are well fitted by the PS formula, and there are massive galaxies in the cluster formation region more than in the field. The summed-up mass function of the cluster galaxies at $z = 0$ has hardly changed from $z \simeq 2$.

4. In the cluster formation region, the number fraction of large galaxies that have undergone mergers for the last 0.5

Gyr is higher than that in the field at high redshift ($z > 3$). After $z \simeq 3$, this fraction in the cluster formation region rapidly decreases and becomes lower than that in the field. In the cluster, merging is the rare event, and only a few massive halos have preferentially merged.

5. A large fraction of the massive halos ($M_h > 10^{11} M_\odot$) at high redshift ($z \simeq 2$) have survived in the cluster at $z \simeq 0.5$. However, after $z \simeq 0.5$ a large fraction of these halos (more than 60% within 0.5 Mpc from the cluster center) are destroyed by the tidal force of the cluster, and the fraction of the surviving halos has a clear correlation with the distance from the cluster center. It is also found that the halos that are stripped in some degree have steeper outer density profiles than the NFW profile, and the halos that have recently accreted into the cluster have density profiles well fitted by the NFW model.

The importance of mergers of individual galaxies to their evolution has been well investigated by numerical simulations (e.g., Barnes 1989) and semianalytic models (e.g., Kauffmann et al. 1993; Cole et al. 1994). Our cluster galaxies merged efficiently at high redshift ($z > 3$). On the other hand, the fraction of the galaxies that have undergone mergers recently (lower z) in the cluster formation region is smaller than that in the field. This difference in the way of merging may explain the difference between observed features of field galaxies and those of cluster galaxies. Furthermore, merging is still important in the cluster at lower z , because it contributes to the increase of mass of the central dominant halo.

In our results, clearly, the most important process that affects the evolution of galactic halos in the cluster is tidal stripping due to the cluster potential. Since tidal stripping diminishes the size of the cluster halos, these halos can hardly merge. Therefore, the summed-up mass function of the cluster galaxies has not changed so much since larger size objects (groups and clusters) formed. A possibility that tidal stripping leads to starbursts and the morphological transformation of galaxies and causes the Butcher-Oemler effect and the density-morphology relation was suggested by Moore et al. (1996b, 1998b). Thus, inclusion of hydrodynamic processes and star formation in our numerical model is very interesting.

For the next step, we will combine our merging history tree of galaxies derived from N -body simulations with population-synthesis models in order to make detailed comparison with the observational data and predictions of semianalytic models. The results of this analysis are given in forthcoming paper.

The authors wish to thank Professor M. Fujimoto, M. Nagashima, and the referee for helpful discussions and comments. Numerical computation in this work was carried out on the HP Exemplar at the Yukawa Institute Computer Facility and on the SGI Origin 2000 at the Division of Physics, Graduate School of Science, Hokkaido University.

REFERENCES

- Aragón-Salamanca, A., Baugh, C. M., & Kauffmann, G. 1998, MNRAS, 297, 427
- Bardeen, J. M., Bond, J. R., Kaiser, N., & Szalay, A. S. 1986, ApJ, 304, 15
- Barnes, J. E. 1989, Nature, 338, 9
- Barnes, J. E., & Hernquist, L. E. 1991, ApJ, 370, L65
- Barnes, J. E., & Hut, P. 1986, Nature, 324, 446
- Baugh, C. M., Cole, S., & Frenk, C. S. 1996, MNRAS, 283, 1361
- Bertschinger, E., & Gelb, J. M. 1991, Comput. Phys., 5, 164
- Binney, J. J., & Tremaine, S. D. 1987, Galactic Dynamics (Princeton: Princeton Univ. Press)
- Bode, P. W., Berrington, R. C., Cohn, H. N., & Lugger, P. M. 1994, ApJ, 433, 479
- Bothun, G. D., & Dressler, A. 1986, ApJ, 301, 57
- Bower, R. G., Lucey, J. R., & Ellis, R. S. 1992, MNRAS, 254, 601

- Butcher, H., & Oemler, A., Jr. 1978, *ApJ*, 219, 18
 ———. 1984a, *ApJ*, 285, 426
 ———. 1984b, *Nature*, 310, 31
 Byrd, G., & Valtonen, M. 1990, *ApJ*, 350, 89
 Carlberg, R. G. 1994, *ApJ*, 433, 468
 Cole, S., Aragón-Salamanca, A., Frenk, C. S., Navarro, J. F., & Zepf, S. E. 1994, *MNRAS*, 271, 781
 Cole, S., & Lacey, C. 1994, *MNRAS*, 271, 676
 Couchman, H. M. P., & Carlberg, R. G. 1992, *ApJ*, 389, 453
 Davis, M., Efstathiou, G., Frenk, C. S., & White, S. D. M. 1985, *ApJ*, 292, 371
 Dressler, A. 1980, *ApJ*, 236, 351
 Ellis, R. S., Smailie, I., Dressler, A., Couch, W. J., Oemler, A., Jr., Butcher, H., & Sharples, R. M. 1997, *ApJ*, 483, 582
 Funato, Y., Makino, J., & Ebisuzaki, T. 1993, *PASJ*, 45, 289
 Gavazzi, G., & Jaffe, W. 1987, *ApJ*, 310, 53
 Gelb, J. M., & Bertschinger, E. 1994, *ApJ*, 436, 467
 Ghigna, S., Moore, B., Governato, F., Lake, G., Quinn, T., & Sadel, J. 1998, *MNRAS*, 300, 146
 Hernquist, L. 1989, *Nature*, 340, 687
 Hernquist, L., & Katz, N. 1989, *ApJS*, 70, 419
 Hoffman, Y., & Ribak, E. 1991, *ApJ*, 380, L5
 Huss, A., Jain, B., & Steinmetz, M. 1997, preprint (astro-ph/9708191)
 Kauffmann, G. 1995a, *MNRAS*, 274, 153
 ———. 1995b, *MNRAS*, 274, 161
 ———. 1996, *MNRAS*, 281, 487
 Kauffmann, G., White, S. D. M., & Guiderdoni, B. 1993, *MNRAS*, 264, 201
 Klypin, A., Gottlöber, S., & Kravtsov, A. V. 1997, preprint (astro-ph/9708191)
 Lacey, C., & Cole, S. 1993, *MNRAS*, 262, 627
 Moore, B., Governato, F., Quinn, T., Stadel, J., & Lake, G. 1998a, *ApJ*, 499, L5
 Moore, B., Katz, N., & Lake, G. 1996a, *ApJ*, 457, 455
 Moore, B., Katz, N., Lake, G., Dressler, A., & Oemler, A. 1996b, *Nature*, 379, 613
 Moore, B., Lake, G., & Katz, N. 1998b, *ApJ*, 495, 139
 Navarro, J. F., Frenk, C. S., & White, S. D. M. 1996, *ApJ*, 462, 563 (NFW)
 Press, W. H., & Schechter, P. 1974, *ApJ*, 187, 425
 Suginohara, T., & Suto, Y. 1992, *ApJ*, 396, 395
 Summers, F. J., Davis, M., & Evrard, A. 1995, *ApJ*, 454, 1
 Suto, Y., Cen, R. Y., & Ostriker, J. P. 1992, *ApJ*, 395, 1
 van Kampen, E. 1995, *MNRAS*, 273, 295
 White, S. D. M. 1976, *MNRAS*, 177, 717
 Whitmore, B. C., Gilmore, D. M., & Jones, C. 1993, *ApJ*, 407, 489